International Journal of Pure and Applied Mathematics
Volume 120 No. 6 2018, 8021-8049
ISSN: 1314-3395 (on-line version)
url: http://www.acadpubl.eu/hub/
Special Issue

http://www.acadpubl.eu/hub/

UNSTEADY MHD FLOW OVER AN INCLINED POROUS PLATE EMBEDDED IN POROUS MEDIUM WITH HEAT ABSORPTION AND SORET-DUFOUR EFFECTS

Siva Reddy Sheri[1], Vijayabhaskar Chathilla[2], D Mahendar[3]
Department of Mathematics,
[1]GITAM University, Hyderabad Campus,
Telangana, India.
[2]Vignan Institute of Technology
Science, Deshhmukhi,
Telangana, India
[3]BVRIT, Narsapur,Medak,Telangana, India
sreddy7@yahoo.co.in

July 17, 2018

Abstract

An analysis is presented to investigate the heat absorption, thermal-diffusion and diffusion- thermo effects on unsteady viscous incompressible MHD flow along semi infinite inclined permeable moving plate with variable temperature and mass diffusion embedded in a porous medium. The governing partial differential equations are formulated and transformed by using a similarity transformation into a system of ordinary differential equations. The resulting equations are solved numerically by finite element method. The numerical results are compared and found to be good agreement with previously published results. The effects of

the various dimensionless parameters entering into the problem on the velocity, temperature and concentration profiles across the boundary layer are investigated through graphs. Also the results of the skin friction coefficient, Nusselt number and Sherwood number at the wall are prepared with various values of the parameters.

***Keywords*:** MHD. Heat Absorption. Soret effect. Dufour effect. Finite Element Method.

1 INTRODUCTION

When heat and mass transfer occur simultaneously in a moving fluid, the relations between the fluxes and the driving potentials are of a more intricate nature. It has been observed that an energy flux can be generated not only by temperature gradients but also by concentration gradients. The energy flux caused by a concentration gradient is termed the diffusion-thermo (Dufour) effect. On the other hand, mass fluxes can also be created by temperature gradients and this embodies the thermal-diffusion (Soret) effect. In most of the studies related to heat and mass transfer process, Soret and Dufour effects are neglected on the basis that they are of a smaller order of magnitude than the effects described by Fouriers and Ficks laws. But these effects are considered as second order phenomena and may become significant in areas such as hydrology, petrology, geosciences, etc. The Soret effect, for instance, has been utilized for isotope separation and in mixture between gases with very light molecular weight (H_2, H_e) and of medium molecular weight (N_2, air). The Dufour effect was recently found to be of order of considerable magnitude so that it cannot be neglected Eckert and Drake [1]. Several other investigators carried out model studies on the Soret and Dufour effects in different heat and mass transfer problems. Some of them are Dursunkaya and Worek [2], Kafoussias and Williams [3], Alam et al. [4] and Srinivasacharya and upendar [5]. Postelnicu [6] analyzed the influence of a magnetic field on heat and mass transfer by natural convection from vertical surface in porous media considering Soret and Dufour effects. Alabraba et al. [7] investigated the interaction of mixed convection with thermal radiation in laminar boundary flow taking into account the binary chemical reaction and Soret-Dufour effects.

Karim et al. [8] investigated Dufour and Soret effect on steady MHD flow in presence of heat generation and magnetic field past an inclined stretching sheet. Recently Pandya and Shukla [9] studied soret-dufour and radiation effect on unsteady MHD flow over an inclined porous plate embedded in porous medium with viscous dissipation. Siva Reddy sheri and srinivasa raju [10] studied Soret effect on unsteady MHD free convective flow past a semi infinite vertical plate in the presence of viscous dissipation.

Soret-Dufour and radiation effect on MHD flows arise in many areas of engineering and applied physics. The study of such flow has application in MHD generators, chemical engineering, nuclear reactors, geothermal energy, reservoir engineering and astrophysical studies. In nature, the assumption of the pure fluid is rather impossible. The presence of foreign mass in the fluid plays an important role in flow of fluid. Thermal diffusion or Soret effect is one of the mechanisms in the transport phenomena in which molecules are transported in a multi-component mixture driven by temperature gradient. The inverse phenomena of thermal diffusion, if multi component mixture were initially at the same temperature, are allowed to diffuse into each other, there arises a difference of temperature in the system. Sparrow and Cess [11] analyzed the effect of magnetic field on free convection heat transfer. Satyanarayana [12] discussed the viscous dissipation and thermal radiation effects on an unsteady MHD convection flow past a semi infinite vertical permeable moving porous plate. Bhattacharya and Dekab [13] studied Radiation and stratification effect on transient free convective flow of an elastico-viscous fluid past an infinite vertical plate. Khem chanda, and Sanjeev Kumar [14], analyzed effect of hall current and rotation on chemically reacting and radiating MHD oscillatory dusty viscoelastic flow through porous vertical channel. Shivaiah and Anand Rao [15] have studied Effects of soret dufour and thermal radiation on an unsteady mhd free convection flow past an infinite vertical porous plate in the presence of chemical reaction. Sivaiah [16] examined MHD flow of a rotating fluid past a vertical porous flat plate in the presence of chemical reaction and radiation. Ravi Kumar [17] explained the effect of the couple stress fluid flow on MHD peristaltic motion with uniform porous medium in the presence of slip effect. Subodh Kumar Sharma et al [18] analyzed computational modeling of temperature field and heat transfer analysis for the piston of

diesel engine with and without air cavity.

Heat absorption/generation effects play a significant role on the heat transfer characteristics of several physical problems of practical interest viz. convection in Earth's mantle, post-accident heat removal, fire and combustion modeling, fluids undergoing exothermic and/or endothermic chemical reaction, development of metal waste from spent nuclear fuel, applications in the field of nuclear energy etc. Therefore, it is appropriate to consider temperature dependent heat source and/or sink which may have strong influence on heat and mass transfer characteristics of the fluid flow problems under consideration. However, exact mathematical modeling of internal heat generation/absorption is highly complicated. It is noticed that some simple mathematical models yet idealized may express their average behavior for most of the physical situations. Sparrow and Cess [19] were one of the initial investigators to consider temperature dependent heat absorption on steady stagnation point flow and heat transfer. Later, several researchers considered hydromagnetic natural convection flow past a flat plate considering different aspects of the problem. Mention may be made of the research studies of Chamkha and Khaled [20]. Jha and Ajibade [21] analyzed natural convection flow of a temperature dependent heat generating/absorbing fluid between vertical porous plates with periodic heat input. Thermal radiation in hydromagnetic flows is an essential aspect of various scenarios in aerospace, mechanical, chemical, environmental and hazards engineering. Industrial applications such as glass production and furnace design, space technology applications such as cosmical flight aerodynamics, rocket propulsion systems and spacecraft re-entry vehicles operate at high temperatures where radiation effects are greatly significant.

The object of the present work is to study effects of heat absorption and Soret-Dufour on unsteady MHD flow over a inclined porous plate embedded in porous medium. Similarity transformation is used to transform the governing partial differential equations to ordinary differential equations which are then solved numerically by finite element method.

2 MATHEMATICAL ANALYSIS

An unsteady flow of a viscous incompressible electrically conducting fluid past an impulsively started infinite inclined porous plate with variable temperature and variable mass diffusion with radiation and viscous dissipation are studied. The physical model and coordinate system are shown in Figure.1. The plate is inclined at angle α to vertical, is embedded in porous medium. x-axis is taken along the plate and y-axis is taken normal to it. It is also considered that the radiation heat flux in direction is negligible in comparison to y-direction. Initially the plate and fluid are at the same temperature T'_∞ and concentration level C'_∞ . At time $t' > 0$, the plate is moving impulsive motion along x' - direction against gravitational field with constant velocity , the plate temperature and concentration raised linearly with time t' . A transverse magnetic field of uniform strength B_0 is assumed normal to the direction of flow. The transversely applied magnetic field and magnetic Reynolds number are very small and hence induced magnetic field is negligible. Due to infinite length in x'-direction, the flow variables are functions of y' and t' only. Under the usual Boussinesq approximation, governing equations are given by

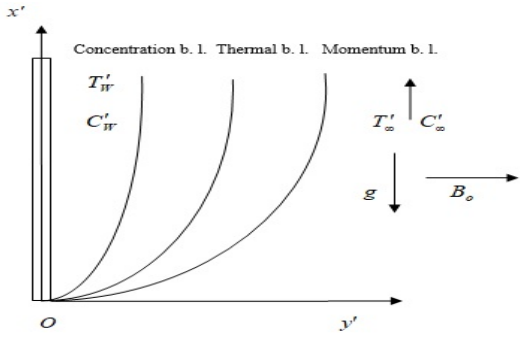

Figure 1: Physical model and coordinate system

Continuity equation:

$$\frac{\partial v'}{\partial y'} = 0 \Rightarrow v' = -v_0 (cons \tan t) \tag{1}$$

Momentum equation:

$$\frac{\partial u'}{\partial t'}+v'\frac{\partial u'}{\partial y'}=\nu\frac{\partial^2 u'}{\partial y'^2}+g\beta(T'-T'_{\infty})\cos(\alpha)+g\beta^*(C'-C'_{\infty})\cos(\alpha)-\frac{\sigma B_0^2 u'}{\rho}-\frac{\nu u'}{K'} \tag{2}$$

Energy equation:

$$\rho C_p\left(\frac{\partial T'}{\partial t'}+v'\frac{\partial T'}{\partial y'}\right)=k\frac{\partial^2 T'}{\partial y'^2}-\frac{\partial q_r}{\partial y'}+\frac{\rho D_m K_T}{C_S}\frac{\partial^2 C'}{\partial y'^2}+\mu\left(\frac{\partial u'}{\partial y'}\right)^2-\frac{Q_0}{\rho C_p}(T'-T'_{\infty}) \tag{3}$$

Equation of continuity for mass transfer

$$\rho C_p\left(\frac{\partial C'}{\partial t'}+v'\frac{\partial C'}{\partial y'}\right)=k\frac{\partial^2 C'}{\partial y'^2}+\frac{\rho D_m K_T}{T_m}\frac{\partial^2 T'}{\partial y'^2} \tag{4}$$

where u' and v' is the velocity component along x'- -direction and y'- direction respectively. g is the acceleration due to gravity, β- is the volumetric coefficient of thermal expansion, β- is the coefficient of volume expansion for mass transfer, v is the kinematic viscosity, μ is viscosity, ρ is the fluid density, B_0 is magnetic induction, K' is the permeability of porous medium, σ is the electrical conductivity of the fluid, T' is the dimensional temperature, T'_{∞} is temperature of free stream, C'_{∞} is concentration of free stream, D_m is the chemical molecular diffusivity, k is the thermal conductivity of the fluid , C_p is specific heat at constant pressure, K'_r is the rate of chemical reaction, K_T is thermal diffusion ratio, C' is the dimensional concentration, q_r is radiative heat flux in y-direction, T_m is mean fluid temperature. Initial and boundary conditions are given as:

$$\begin{aligned} &t'\le 0 \;\; u'=0 \;\; T'=T'_{\infty} \;\; C'=C'_{\infty} \;\; for \;\; all \;\; y' \\ &t'>0 \;\; \begin{cases} u'=u_0 \;\; v'=-v_0 \;\; T'=T'+(T'_w-T'_{\infty})e^{At'} \;\; C'=C'+(C'_w-C'_{\infty})e^{At'} \;\; as \;\; y'=0 \\ u'=0, \;\; T'\to\infty, \; C'\to\infty \;\; as \;\; y'\to\infty \end{cases} \end{aligned} \tag{5}$$

where

$$A = \frac{V_0^2}{\nu} \text{A=, } T'_w \text{ and } C'_w$$

are temperature and concentration of plate respectively. The radiative heat flux term by using the Roseland approximation is given by

$$q_r = \frac{-4\sigma}{3K_1}\frac{\partial T'^4}{\partial y'} \tag{6}$$

where K_1 and σ are mean absorption coefficient and Stefan Boltzmann constant respectively. It is assumed that the temperature difference within the flow are sufficiently small such that T'^4 may be expressed as a linear function of the temperature. This is accomplished by expanding in a Taylor series about T'_∞ and neglecting the higher order terms, thus

$$T'^4 \cong 4T'^3_\infty T' - 3T'^4_\infty \tag{7}$$

then using Eqs. (6) and (7), Eq. (3) is reduced

$$\rho C_p\left(\frac{\partial T'}{\partial t'} + v'\frac{\partial T'}{\partial y'}\right) = k\frac{\partial^2 T'}{\partial y'^2} + \frac{16\sigma T'^3_\infty}{3K_1}\frac{\partial^2 T'}{\partial y'^2} + \frac{\rho D_m K_T}{C_s}\frac{\partial^2 C'}{\partial y'^2} + \mu\left(\frac{\partial u'}{\partial y'}\right)^2 - \frac{Q_0}{\rho C_p}(T' - T'_\infty) \tag{8}$$

In order to acquire non-dimensional partial differential equations, introducing following dimensionless quantities:

In order to write the governing equations and the boundary conditions in dimensionless form, the following non dimensional quantities are introduced.

$$\left.\begin{aligned} &u=\frac{u'}{u_o},\ t=\frac{t'v_0^2}{\nu},\ y=\frac{v_o y'}{\nu},\ \Pr=\frac{\mu C_p}{k},\ \theta=\frac{T'-T'_\infty}{T'_w-T'_\infty},\ \phi=\frac{C'-C'_\infty}{C'_w-C'_\infty},\ K=\frac{K'v_o^2}{\nu^2},\\ &Gr=\frac{g\beta\nu(T'_w-T'_\infty)}{u_o v_o^2},\ Gm=\frac{\nu g\beta^*(C'_w-C'_\infty)}{u_o v_o^2},\ Du=\frac{D_m K_T(C'_w-C'_\infty)}{C_S C_P\nu(T'_w-T'_\infty)}\ Sr=\ \frac{D_m K_T(T'_w-T'_\infty)}{T_m\nu(C'_w-C'_\infty)},\\ &M=\frac{\sigma B_o^2\nu}{\rho v_o^2},\ R=\frac{4\sigma T'^3_\infty}{k_1 k},\ Sc=\frac{\nu}{D_m},\ Q=\frac{Q_0\nu}{\rho C_p v_0^2},\ E_C=\frac{u_o^{\ 2}}{C_p(T'_w-T'_\infty)} \end{aligned}\right\} \tag{9}$$

Introducing Eq. (9), we obtain non-dimensional form of Eqs. (2), (8) and (4) respectively:

$$\frac{\partial u}{\partial t}-\frac{\partial u}{\partial y}=Gr\theta\cos\alpha+Gm\phi\cos\alpha+\frac{\partial^2 u}{\partial y^2}-(M+\frac{1}{K})u \tag{10}$$

$$\frac{\partial\theta}{\partial t}-\frac{\partial\theta}{\partial y}=\frac{1}{\Pr}\left[1+\frac{4R}{3}\right]\frac{\partial^2\theta}{\partial y^2}+Du\frac{\partial^2\phi}{\partial y^2}+E_c\left(\frac{\partial u}{\partial y}\right)^2-Q\theta \tag{11}$$

$$\frac{\partial\phi}{\partial t}-\frac{\partial\phi}{\partial y}=\frac{1}{Sc}\frac{\partial^2\phi}{\partial y^2}+Sr\frac{\partial^2\theta}{\partial y^2} \tag{12}$$

The corresponding dimensionless boundary conditions are:

$$\left.\begin{aligned} &t\le 0:\quad u=0,\ \theta=0,\ \phi=0\quad for\ \ all\quad y\\ &t>0:\quad \begin{cases} u=1,\ \theta=e^t,\ \phi=e^t\ \ as\quad y=0\\ u=0\quad u\to 0\quad \phi\to 0\ \ as\quad y\to 0 \end{cases} \end{aligned}\right\} \tag{13}$$

Now it is important to calculate the physical quantities of primary interest, which are the local shear stress, local surface heat flux and Sherwood number. Dimensionless local wall shear stress or skin-friction is obtained as,

$$\tau = \frac{\tau_w}{\rho u_w^2}, \quad \tau_w = \left[\mu \frac{\partial u'}{\partial y'}\right]_{y'=0} = \rho U_o^2 u'(0) = \left[\frac{\partial u}{\partial y}\right]_{y=0} \tag{14}$$

The dimensionless local surface heat flux (i.e., Nusselt number) is obtained as then

$$N_u(x') = -\left[\frac{x'}{(T_w' - T_\infty')} \frac{\partial T'}{\partial y'}\right]_{y'=0} \quad \text{then} \quad Nu = -\frac{N_u(x')}{R_{e_x}} = -\left[\frac{\partial \theta}{\partial y}\right]_{y=0} \tag{15}$$

The definition of the local mass flux and the local Sherwood number are respectively given by with the help of these equations, one can write

$$S_h(x') = -\left[\frac{x'}{(C_w' - C_\infty')} \frac{\partial C'}{\partial y'}\right]_{y'=0} \quad \text{then} \quad Sh = -\frac{S_h(x')}{R_{e_x}} = -\left[\frac{\partial \phi}{\partial y}\right]_{y=0} \tag{16}$$

Where

$$R_{e_x} = \frac{U_o x'}{\nu},$$

is the Reynolds number.

3 METHOD OF SOLUTION

The finite element method has been implemented to obtain numerical solutions of equations (10)-(12) under boundary conditions (13). This technique is extremely efficient and allows robust solutions of complex coupled, nonlinear multiple degree differential equation systems. The fundamental steps comprising the method are now summarized. An excellent description of finite element formulations is available in Bathe [22] and Reddy [23].

Step-1: Discretization of the Domain into Elements

The whole domain is divided into finite number of sub-domains, a process known as Discretization of the domain. Each sub-domain is termed a finite element. The collection of elements is designated the finite element mesh.

Step-2: Derivation of the element Equations

The derivation of finite element equations algebraic equations among the unknown parameters of the finite element approximation, involves the following three steps.

a. Construct the variational formulation of the differential equation.

b. Assume the form of the approximate solution over a typical finite element.

c. Derive the finite element equations by substituting the approximate solution into variational formulation.

These steps results in a matrix equation of the form , which defines the finite element model of the original equation.

Step-3: Assembly of Element Equations

The algebraic equations so obtained are assembled by imposing the inter-element continuity conditions. This yields a large number of algebraic equations constituting the global finite element model, which governs the whole flow domain.

Step-4: Impositions of Boundary Conditions

The physical boundary conditions defined in (13) are imposed on the assembled equations

Step-5: Solution of the Assembled Equations

The final matrix equation can be solved by a direct or indirect (iterative) method. For computational purposes, the coordinate is varied from to , where represents infinity external to the momentum, energy and concentration boundary layers. The whole domain is divided into a set of line segments of equal width each element being two-noded.

Variational formulation

The variational formulation associated with equations (10) (12) over a typical two noded linear element (y_e, y_{e+1}) is given by

$$\int_{y_e}^{y_{e+1}} w_1\left[\left(\frac{\partial u}{\partial t}\right)-\left(\frac{\partial u}{\partial y}\right)-\left(\frac{\partial^2 u}{\partial y^2}\right)+Nu-Gr\theta\cos\alpha-Gm\phi\cos\alpha\right]dy=0 \tag{17}$$

$$\int_{y_e}^{y_{e+1}} w_2\left[\left(\frac{\partial \theta}{\partial t}\right)-\left(\frac{\partial \theta}{\partial y}\right)-\frac{1}{\Pr}\left[1+\frac{4R}{3}\right]\left(\frac{\partial^2 \theta}{\partial y^2}\right)-Du\frac{\partial^2 \phi}{\partial y^2}-E_c\left(\frac{\partial u}{\partial y}\right)^2-Q\theta\right]dy=0 \tag{18}$$

$$\int_{y_e}^{y_{e+1}} w_3\left[\left(\frac{\partial \phi}{\partial t}\right)-\left(\frac{\partial \phi}{\partial y}\right)-\frac{1}{Sc}\left(\frac{\partial^2 \phi}{\partial y^2}\right)-Sr\frac{\partial^2 \theta}{\partial y^2}\right]dy=0 \tag{19}$$

Where w_1, w_2, w_3 are arbitrary test functions and may be viewed as the variation in u,θ and ϕ respectively. After reducing the order of integration and non linearity, we arrive at the following system of equations.

$$\int_{y_e}^{y_{e+1}}\left[(w_1)\left(\frac{\partial u}{\partial t}\right)-\left(\frac{\partial u}{\partial y}\right)+\left(\frac{\partial w_1}{\partial y}\right)\left(\frac{\partial u}{\partial y}\right)+N(w_1)u-(Gr)(w_1)\theta\cos\alpha-(Gm)(w_1)\phi\cos\alpha\right]dy$$
$$-\left[(w_1)\left(\frac{\partial u}{\partial y}\right)\right]_{y_e}^{y_{e+1}}=0 \tag{20}$$

$$\int_{y_e}^{y_{e+1}}\left[(w_2)\left(\frac{\partial \theta}{\partial t}\right)-(w_2)\left(\frac{\partial \theta}{\partial y}\right)+\frac{1}{\Pr}\left[1+\frac{4R}{3}\right]\left(\frac{\partial w_2}{\partial y}\right)\left(\frac{\partial \theta}{\partial y}\right)-Du\left(\frac{\partial w_2}{\partial y}\right)\left(\frac{\partial \phi}{\partial y}\right)-E_c(w_2)\left(\frac{\partial \bar{u}}{\partial y}\right)\left(\frac{\partial u}{\partial y}\right)\right]dy$$
$$-\left[\left(\frac{w_2}{\Pr}\right)\left[1+\frac{4R}{3}\right]\left(\frac{\partial \theta}{\partial y}\right)-(Du)w_2\left(\frac{\partial \phi}{\partial y}\right)-Q(w_2)\theta\right]_{y_e}^{y_{e+1}}=0 \tag{21}$$

$$\int_{y_e}^{y_{e+1}} \left[(w_3)\left(\frac{\partial \phi}{\partial t}\right) - B(w_3)\left(\frac{\partial \phi}{\partial y}\right) + \frac{1}{Sc}\left(\frac{\partial w_3}{\partial y}\right)\left(\frac{\partial \phi}{\partial y}\right) - (Sr)\left(\frac{\partial w_3}{\partial y}\right)\left(\frac{\partial \phi}{\partial y}\right)\right] dy$$
$$- \left[\left(\frac{w_3}{Sc}\right)\left(\frac{\partial \phi}{\partial y}\right) - (Sr)(w_3)\left(\frac{\partial \phi}{\partial y}\right)\right]_{y_e}^{y_{e+1}} = 0 \tag{22}$$

Finite Element formulation: The finite element model may be obtained from equations (20) (22) by substituting finite element approximations of the form:

$$u = \sum_{j=1}^{2} u_j^e \psi_j^e, \quad \theta = \sum_{j=1}^{2} \theta_j^e \psi_j^e, \quad \phi = \sum_{j=1}^{2} \phi_j^e \psi_j^e \tag{23}$$

With $w_1 = w_2 = w_3 = \psi_j^e (i = 1, 2)$, where $u_j^e, \theta_j^e and \phi_j^e$ are the velocity, temperature and concentration respectively at the jth node of typical eth element (y_e, y_{e+1}) and ϕ_i^e are the shape functions for this element (y_e, y_{e+1}) and are taken as:

$$\psi_1^e = \frac{y_{e+1} - y}{y_{e+1} - y_e} \text{ and } \psi_2^e = \frac{y - y_e}{y_{e+1} - y_e}, \; y_e \le y \le y_{e+1} \tag{24}$$

The finite element model of the equations for element thus formed is given by

$$\begin{bmatrix} [K^{11}] & [K^{12}] & [K^{13}] \\ [K^{21}] & [K^{22}] & [K^{23}] \\ [K^{31}] & [K^{32}] & [K^{33}] \end{bmatrix} \begin{bmatrix} \{u^e\} \\ \{\theta^e\} \\ \{\phi^e\} \end{bmatrix} + \begin{bmatrix} [M^{11}] & [M^{12}] & [M^{13}] \\ [M^{21}] & [M^{22}] & [M^{23}] \\ [M^{31}] & [M^{32}] & [M^{33}] \end{bmatrix} \begin{bmatrix} \{u'^e\} \\ \{\theta'^e\} \\ \{\phi'^e\} \end{bmatrix} = \begin{bmatrix} \{b^{1e}\} \\ \{b^{2e}\} \\ \{b^{3e}\} \end{bmatrix} \tag{25}$$

Where

$$\{K^{mn}\}, \{M^{mn}\} \text{ and } \{\{u^e\}, \{\theta^e\}, \{\phi^e\}, \{u'^e\}, \{\theta'^e\}, \{\phi'^e\} and \{b^{me}\}\}(m, n = 1, 2, 3)$$

are the set of matrices of order 2x1 and 2x2 respectively and (dash) indicates d/dy . These matrices are defined as follows:

$$K_{ij}^{11}=-\int_{y_e}^{y_{e+1}}\left[\left(\psi_i^e\right)\left(\frac{\partial\psi_j^e}{\partial y}\right)\right]dy+\int_{y_e}^{y_{e+1}}\left[\left(\frac{\partial\psi_i^e}{\partial y}\right)\left(\frac{\partial\psi_j^e}{\partial y}\right)\right]dy+N\int_{y_e}^{y_{e+1}}\left[\left(\psi_i^e\right)\left(\psi_j^e\right)\right]dy,\ K_{ij}^{12}=-\int_{y_e}^{y_{e+1}}\left(\psi_i^e\right)dy,$$

$$K_{ij}^{13}=-\left[Gr\cos\alpha+Gm\cos\alpha\right]\int_{\eta_e}^{\eta_{e+1}}\left(\psi_i^e\right)\left(\psi_j^e\right)dy,\ M_{ij}^{11}=\int_{y_e}^{y_{e+1}}\left(\psi_i^e\right)\left(\psi_j^e\right)dy,\ M_{ij}^{12}=M_{ij}^{13}=0,$$

$$K_{ij}^{21}=-(Ec)\int_{y_e}^{y_{e+1}}\left(\psi_i^e\right)\left(\frac{\partial\overline{u}}{\partial y}\right)\left(\frac{\partial\psi_j^e}{\partial y}\right)dy,\ K_{ij}^{22}=-\int_{y_e}^{y_{e+1}}\left[\left(\psi_i^e\right)\left(\frac{\partial\psi_j^e}{\partial y}\right)\right]dy+\frac{1}{\Pr}\left[1+\frac{4R}{3}\right]\int_{y_e}^{y_{e+1}}\left[\left(\frac{\partial\psi_i^e}{\partial y}\right)\left(\frac{\partial\psi_j^e}{\partial y}\right)\right]dy,$$

$$K_{ij}^{23}=S\int_{y_e}^{y_{e+1}}\left[\left(\psi_i^e\right)\left(\psi_j^e\right)\right]dy-Du\int_{y_e}^{y_{e+1}}\left(\frac{\partial\psi_i^e}{\partial y}\right)\left(\frac{\partial\psi_j^e}{\partial y}\right)dy--Q\int_{y_e}^{y_{e+1}}\left(\psi_i^e\right)\left(\psi_j^e\right)dy,\ M_{ij}^{21}=M_{ij}^{23}=0,$$

$$M_{ij}^{22}=\int_{y_e}^{y_{e+1}}\left(\psi_i^e\right)\left(\psi_j^e\right)dy,\ M_{ij}^{31}=M_{ij}^{32}=0,\ M_{ij}^{33}=\int_{y_e}^{y_{e+1}}\left(\psi_i^e\right)\left(\psi_j^e\right)dy,\ K_{ij}^{31}=0,\ K_{ij}^{32}=-\left[(Sr)\int_{y_e}^{y_{e+1}}\left(\frac{\partial\psi_i^e}{\partial y}\right)\left(\frac{\partial\psi_j^e}{\partial y}\right)dy\right],$$

$$K_{ij}^{33}=-\int_{y_e}^{y_{e+1}}\left[\left(\psi_i^e\right)\left(\frac{\partial\psi_j^e}{\partial y}\right)\right]dy+\frac{1}{Sc}\int_{y_e}^{y_{e+1}}\left[\left(\frac{\partial\psi_i^e}{\partial y}\right)\left(\frac{\partial\psi_j^e}{\partial y}\right)\right]dy,\ b_i^{1e}=\left[\left(\psi_i^e\right)\left(\frac{\partial u}{\partial y}\right)\right]_{y_e}^{y_{e+1}},$$

$$b_i^{2e}=\left[\left(\frac{\psi_i^e}{\Pr}\right)\left(\frac{\partial\theta}{\partial y}\right)-(Du)\left(\psi_i^e\right)\left(\frac{\partial\phi}{\partial y}\right)\right]_{y_e}^{y_{e+1}},\ b_i^{3e}=\left[\left(\frac{\psi_i^e}{Sc}\right)\left(\frac{\partial\phi}{\partial y}\right)-(Sr)\left(\psi_i^e\right)\left(\frac{\partial\theta}{\partial y}\right)\right]_{y_e}^{y_{e+1}}$$

The whole domain is divided into a set of 60 intervals of equal length 0.1. At each node 3 functions are to be evaluated. Hence after assembly of the elements we obtain a set of 143 equations. The system of equations after assembly of elements, are non-linear and consequently an iterative scheme is employed to solve the matrix system, which are solved using the Gauss Elimination method maintaining an accuracy of 0.0005.

4 RESULTS AND DISCUSSIONS

In this section, a representative set of numerical results for the velocity, temperature and concentration profiles shown graphically

in Figures 2-20. The following parameter values are adopted for computations unless otherwise indicated in the figures and table:

$$Gr = 5.0, Gm = 10.0, \alpha = 30, M = 5.0, K = 1.0,$$

$$\Pr = 0.71, R = 2.0, Ec = 1.0, \ Sr = 1.0 \ Du \ = 0.7, \ Sc \ = 0.66, Q \ = 1.0, t = 0.2$$

To assess the accuracy of the present method, comparisons between the present results and previously published data Pandya and Shukla [9], Table 1 shows the comparison between values of skin-friction coefficient τ. Table 2 shows the comparison between values of Nusselt number of Nu, also Table 3 shows the comparison between values of Sherwood number Sh . In fact, these results are good agreement.

For the case of different thermal Grashof numbers Gr , the velocity profiles in the boundary layer are shown in Fig. 2. As expected, it is observed that an increase in Gr leads to the decrease in the velocity due to the enhancement in the buoyancy force. Here, the positive values of Gr correspond to the cooling surface. In addition, the curves show that the peak values of the velocity decrease rapidly near the wall of the porous plate as Gr increases, and then decay to the free stream velocity. Figure 3 presents the typical velocity profiles in the boundary layer for various solutal Grash of numbers Gm with the same other parameters as before. It is seen that the velocity distribution attains a distinctive maximum value in the vicinity of the plate surface, and then decreases properly to approach the free stream value. As expected, the fluid velocity increases, and the peak value is much distinctive due to the increase in the concentration buoyancy effects represented by Gm. This is evident in the increase in u as Gm increases. The velocity profiles for different values of inclination angle α are given in Fig. 4. It is observed that an increase in α leads to a fall in the values of the velocity. In addition, the curves show that the peak value of the velocity near the wall of the porous plate decreases rapidly with *alpha*. The velocity profiles for different values of the magnetic field parameter are plotted in Fig. 5. It is obvious that an increase in the value of results in a decrease in the velocity in the boundary layer. This is due to the fact that the introduction of a transverse

magnetic field, normal to the flow direction, has a tendency to create the drag known as the Lorentz force which tends to resist the flow. The profiles of the velocity in the boundary layer for various values of the permeability are shown in Fig. 6. It is seen that the peak value of the velocity near the wall of the porous plate increases rapidly with , and then the velocity decays to the relevant free stream value.

Figures 7 and 8 illustrate the velocity and temperature profiles for different Prandtl numbers . The results show that the increasing Prandtl number results in an increase in the velocity, and an increase in the Prandtl number results in a decrease in the thermal boundary layer and in general lower average temperature within the boundary layer. The reason is that smaller is equivalent to the increase in the thermal conductivity of the fluid, and heat is able to diffuse away from the heated surface more rapidly for higher values of . Therefore, in the case of smaller Prandtl numbers, the thermal boundary layer is thicker, and the rate of heat transfer is reduced.

The velocity profiles are plotted in Figure 9. Here, as the value of R increases the velocity increases, with an increasing in the flow boundary layer thickness. Thus, thermal radiation enhances convective flow. The effects of radiation parameter R on the temperature profiles are presented in Figure 10. From this figure we observe that, as the value of R increases the temperature profiles increases, with an increasing in the thermal boundary layer thickness.

The effects of the viscous dissipation parameter, i.e., the Eckert number Ec, on the velocity and temperature are shown in Figs. 11and 12, respectively. The Eckert number Ec, expresses the relationship between the kinetic energy in the flow and the enthalpy. It embodies the conversion of kinetic energy into internal energy by work done against the viscous fluid stresses. Greater viscous dissipative heat causes a rise in the temperature as well as the velocity. This behavior is evident from Figs. 11and 12. For various values of the Dufour number Du, the velocity and temperature profiles are plotted in Figs 13 and 14 respectively. The Dufour number Du denotes the contribution of the concentration gradients to the thermal energy flux in the flow. It can be seen that an increase in the Dufour number causes a rise in the velocity and temperature throughout the boundary layer. For, the temperature profiles decay smoothly from the plate to the free stream value. However for, a

distinct velocity overshoot exists near the plate, and thereafter the profile falls to zero at the edge of the boundary layer.

Figs 15 and 16 show the velocity and temperature profiles for different heat source parameters Q. As shown in Fig. 15, the increasing heat source parameter Q decreases the boundary layer. It is due to the fact that when heat is absorbed, the buoyancy force decreases and retards the flow rate, which, thereby, gives rise to the decrease in the velocity profiles. From Fig. 16, we observe that the temperature decreases with the increase in the heat source parameter Q because when heat is absorbed, the buoyancy force decreases the temperature profiles.

Figs 17 and 18 display the velocity and concentration profiles for different values of the Soret number Sr. The Soret number defines the effect of the temperature gradients inducing significant mass diffusion effects. It is noticed that an increase in the Soret number Sr results in an increase in the velocity and concentration within the boundary layer.

Figs 19 and 20 show the velocity and concentration profiles across the boundary layer for various values of the Schmidt number Sc . The Schmidt number is the ratio of the momentum diffusivity to the mass (species) diffusivity, i.e., it relates the thickness of the hydrodynamic boundary layer to that of the mass transfer (concentration) boundary layer. The figure shows that an increase in Sc results in a decrease in the velocity and concentration, because smaller values of Sc are equivalent to an increasing chemical molecular diffusivity.

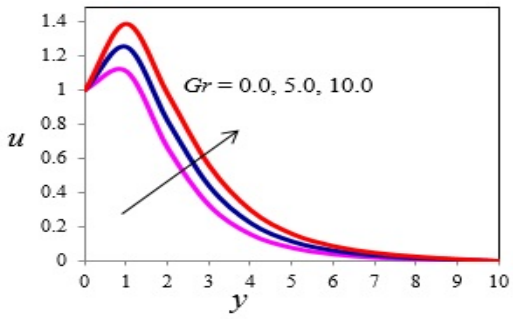

Figure 2. Velocity profiles for different values of Gr

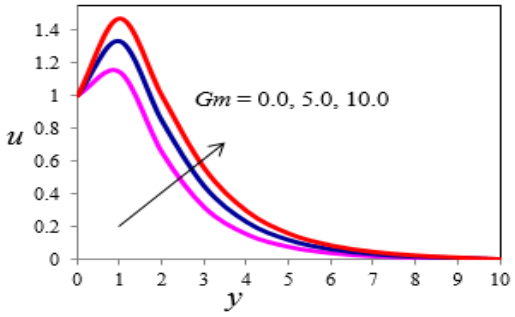

Figure 3. Velocity profiles for different values of Gm

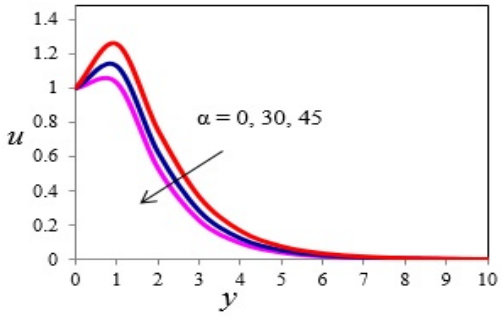

Figure 4. Velocity profiles for different values of α

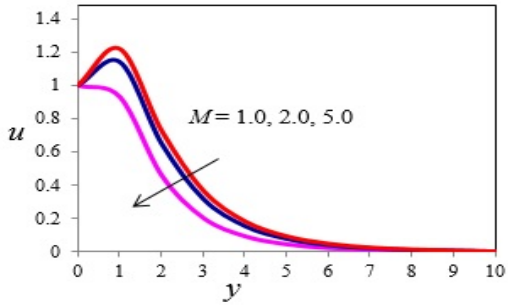

Figure 5. Velocity profiles for different values of M

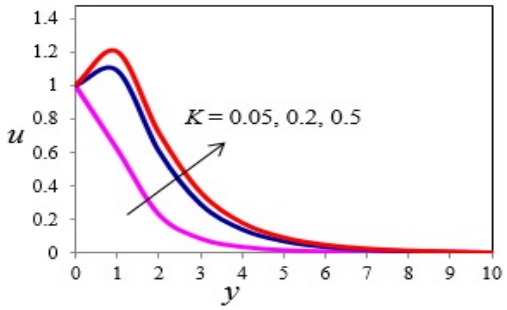

Figure 6. Velocity profiles for different values of K

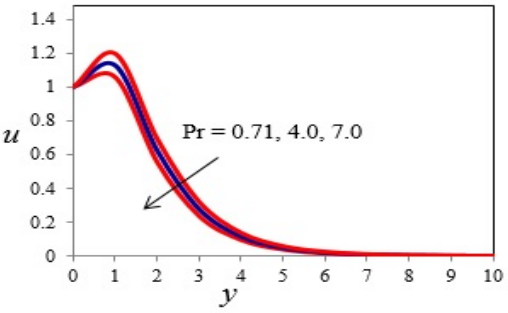

Figure 7. Velocity profiles for different values of Pr

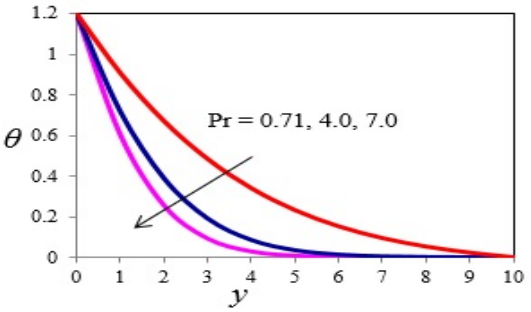

Figure 8. Temperature profiles for different values of Pr

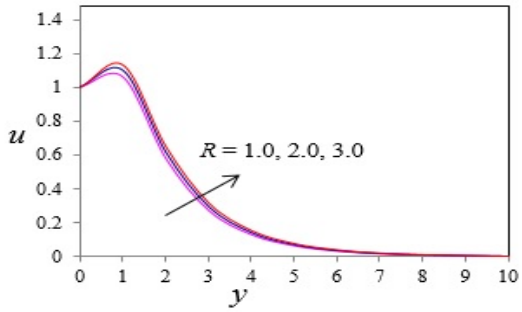

Figure 9. Velocity profiles for different values of R

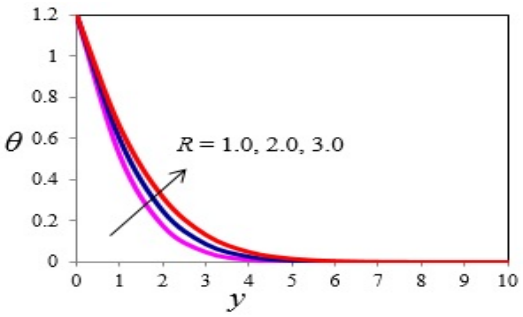

Figure 10. Temperature profiles for different values of R

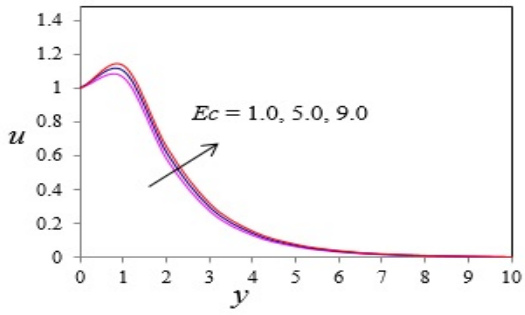

Figure 11. Velocity profiles for different values of Ec

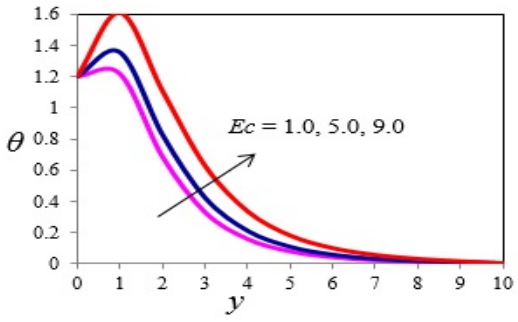

Figure 12. Temperature profiles for different values of Ec

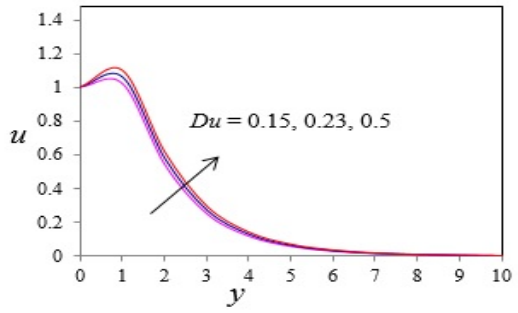

Figure 13. Velocity profiles for different values of Du

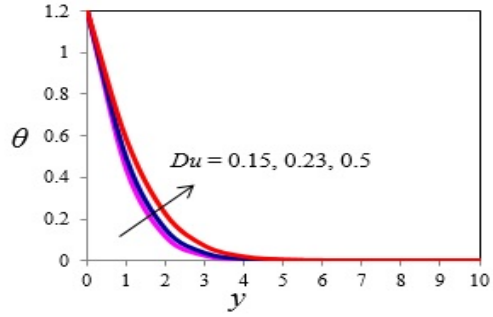

Figure 14. Temperature profiles for different values of Du

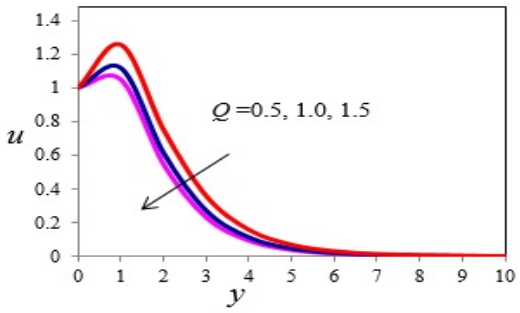

Figure 15. Velocity profiles for different values of Q

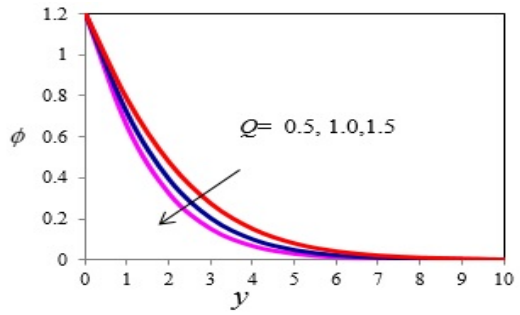

Figure 16. Temperature profiles for different values of Q

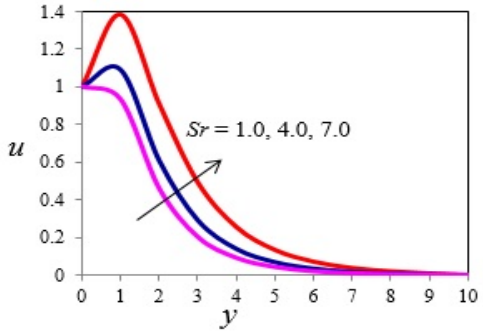

Figure 17. Velocity profiles for different values of Sr

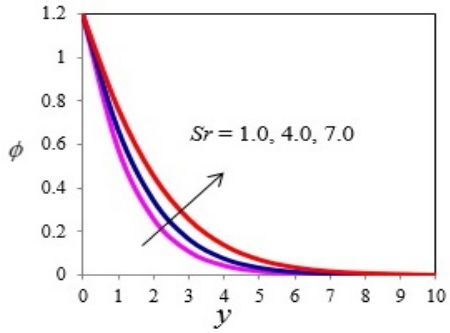

Figure 18. Concentration profiles for different values of Sr

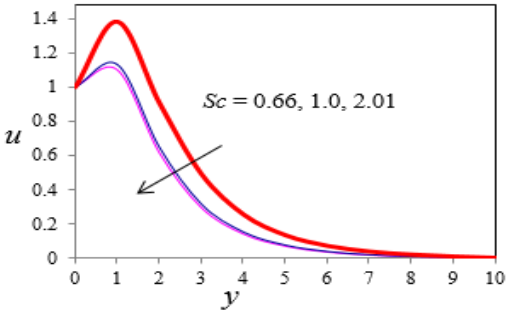

Figure 19. Velocity profiles for different values of Sc

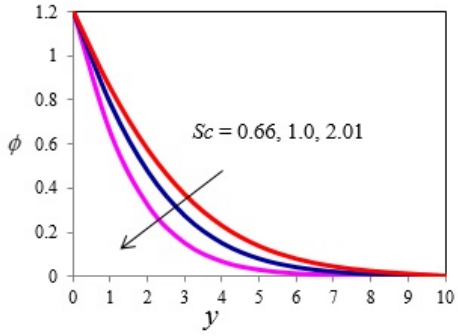

Figure 20. Concentration profiles for different values of Sc

Table 1 displays that enhancing thermal Grashof number Gr , solutal Grashof number Gm , ,permeability parameter K , Dufour number Du, Soret number Sr , Eckert number Ec , Radiation parameter R and time t , skin-friction coefficient increases. And increasing inclination angle α , magnetic parameter M , Prandtl number Pr and Schmidt number Sc , skin-friction coefficient decreases. Table 2 shows that raising Dufour number Du , Soret number Sr , Prandtl number Pr , Nusselt number Nu increases. Increasing inclination angle α , Eckert number Ec , radiation parameter R, Schmidt number Sc , time t , Nusselt number Nu decreases. Table 3 exhibits that increasing Radiation parameter R, Eckert number Ec , Schmidt number Sc, inclination angle α, Sherwood number Sh increases. Enhancing Dufour number Du, Prandtl number Pr , Soret number Sr , time t , Sherwood number Sh decreases.

Table 1. skin friction coefficient for different values of parameters ($Q = 0.0$)

t	R	Pr	M	K	Sc	Sr	α	Du	Gm	Gr	Ec	Pandya and Shukla [9] results τ	Present results τ
0.2	1.0	0.71	5.0	1.0	0.66	1.0	30.0	0.7	10.0	5.0	1.0	0.458197	0.458197
0.2	3.0	0.71	5.0	1.0	0.66	1.0	30.0	0.7	10.0	5.0	1.0	0.523628	0.523628
0.2	2.0	4.0	5.0	1.0	0.66	1.0	30.0	0.7	10.0	5.0	1.0	0.372707	0.372707
0.2	2.0	7.0	5.0	1.0	0.66	1.0	30.0	0.7	10.0	5.0	1.0	0.351861	0.351861
0.2	2.0	0.71	1.0	1.0	0.66	1.0	30.0	0.7	10.0	5.0	1.0	1.60966	1.60966
0.2	2.0	0.71	2.0	1.0	0.66	1.0	30.0	0.7	10.0	5.0	1.0	1.29914	1.29914
0.2	2.0	0.71	5.0	0.5	0.66	1.0	30.0	0.7	10.0	5.0	1.0	0.264523	0.264523
0.2	2.0	0.71	5.0	0.8	0.66	1.0	30.0	0.7	10.0	5.0	1.0	0.436886	0.436886
0.2	2.0	0.71	5.0	1.0	1.0	1.0	30.0	0.7	10.0	5.0	1.0	0.287898	0.287898
0.2	2.0	0.71	5.0	1.0	3.0	1.0	30.0	0.7	10.0	5.0	1.0	-0.307713	-0.307713
0.2	2.0	0.71	5.0	1.0	0.66	4.0	30.0	0.7	10.0	5.0	1.0	0.883421	0.883421
0.2	2.0	0.71	5.0	1.0	0.66	7.0	30.0	0.7	10.0	5.0	1.0	1.40196	1.40196
0.2	2.0	0.71	5.0	1.0	0.66	1.0	0.0	0.7	10.0	5.0	1.0	0.976127	0.976127
0.2	2.0	0.71	5.0	1.0	0.66	1.0	60.0	0.7	10.0	5.0	1.0	-0.812158	-0.812158
0.2	2.0	7.0	5.0	1.0	0.66	1.0	30.0	0.15	10.0	5.0	1.0	0.322698	0.322698
0.2	2.0	7.0	5.0	1.0	0.66	1.0	30.0	0.23	10.0	5.0	1.0	0.326735	0.326735
0.2	2.0	0.71	5.0	1.0	0.66	1.0	30.0	0.7	0	5.0	1.0	-1.3527	-1.3527
0.2	2.0	0.71	5.0	1.0	0.66	1.0	30.0	0.7	15	5.0	1.0	1.42055	1.42055
0.2	2.0	0.71	5.0	1.0	0.66	1.0	30.0	0.7	10.0	0.0	1.0	-0.753363	-0.753363
0.2	2.0	0.71	5.0	1.0	0.66	1.0	30.0	0.7	10.0	15.0	1.0	3.01956	3.01956
0.2	2.0	0.71	5.0	1.0	0.66	1.0	30.0	0.7	10.0	5.0	9.0	0.571954	0.571954
0.2	2.0	0.71	5.0	1.0	0.66	1.0	30.0	0.7	10.0	5.0	14.0	0.615956	0.615956
0.3	2.0	0.71	5.0	1.0	0.66	1.0	30.0	0.7	10.0	5.0	1.0	1.31261	1.31261
0.4	2.0	0.71	5.0	1.0	0.66	1.0	30.0	0.7	10.0	5.0	1.0	2.01698	2.01698

Table2. Nusselt number for different values of parameters ($Q = 0.0, M = 5.0, K = 1.0, Gm = 10.0, Gr = 5.0$)

t	R	Pr	Sc	Sr	α	Du	Ec	Pandya and Shukla [9] results Nu	Present results Nu
0.2	1.0	0.71	0.66	1.0	30.0	0.7	1.0	0.823538	0.823538
0.2	3.0	0.71	0.66	1.0	30.0	0.7	1.0	0.585463	0.585463
0.2	2.0	4.0	0.66	1.0	30.0	0.7	1.0	1.6441	1.6441
0.2	2.0	7.0	0.66	1.0	30.0	0.7	1.0	2.83998	2.83998
0.2	2.0	0.71	1.0	1.0	30.0	0.7	1.0	0.60778	0.60778
0.2	2.0	0.71	2.01	1.0	30.0	0.7	1.0	0.440804	0.440804
0.2	2.0	0.71	3.0	4.0	30.0	0.7	1.0	0.750167	0.750167
0.2	2.0	0.71	0.66	7.0	30.0	0.7	1.0	0.866699	0.866699
0.2	2.0	7.0	0.66	1.0	30.0	0.15	1.0	2.65431	2.65431
0.2	2.0	7.0	0.66	1.0	30.0	0.23	1.0	2.66072	2.66072
0.2	2.0	0.71	0.66	1.0	0.0	0.7	1.0	0.668204	0.668204
0.2	2.0	0.71	0.66	1.0	60.0	0.7	1.0	0.661289	0.661289
0.2	2.0	0.71	0.66	1.0	30.0	0.7	5.0	0.348693	0.348693
0.2	2.0	0.71	0.66	1.0	30.0	0.7	9.0	0.0553734	0.0553734
0.1	2.0	0.71	0.66	1.0	30.0	0.7	1.0	0.753282	0.753282
0.3	2.0	0.71	0.66	1.0	30.0	0.7	1.0	0.661833	0.661833

Table 3. Sherwood number for different values of parameters ($Q = 0.0, M = 5.0, K = 1.0, Gm = 10.0, Gr = 5.0$)

t	R	Pr	Sc	Sr	α	Du	Ec	Pandya and Shukla [9] results Sh	Present results Sh
0.2	1.0	0.71	0.66	1.0	30.0	0.7	1.0	1.61099	1.61099
0.2	3.0	0.71	0.66	1.0	30.0	0.7	1.0	1.69869	1.69869
0.2	2.0	4.0	0.66	1.0	30.0	0.7	1.0	1.20522	1.20522
0.2	2.0	7.0	0.66	1.0	30.0	0.7	1.0	0.514665	0.514665
0.2	2.0	0.71	1.0	1.0	30.0	0.7	1.0	2.15851	2.15851
0.2	2.0	0.71	2.01	1.0	30.0	0.7	1.0	3.44766	3.44766
0.2	2.0	0.71	0.66	4.0	30.0	0.7	1.0	1.11221	1.11221
0.2	2.0	0.71	0.66	10.0	30.0	0.7	1.0	-2.26392	-2.26392
0.2	2.0	7.0	0.66	1.0	30.0	0.15	1.0	0.654562	0.654562
0.2	2.0	7.0	0.66	1.0	30.0	0.23	1.0	0.646871	0.646871
0.2	2.0	0.71	0.66	1.0	0.0	0.7	1.0	1.66869	1.66869
0.2	2.0	0.71	0.66	1.0	60.0	0.7	1.0	1.68041	1.68041
0.2	2.0	0.71	0.66	1.0	30.0	0.7	5.0	1.822	1.822
0.2	2.0	0.71	0.66	1.0	30.0	0.7	9.0	1.96107	1.96107
0.1	2.0	0.71	0.66	1.0	30.0	0.7	1.0	1.8813	1.8813

5 CONCLUSION

This work studied the heat absorption and soret-dufour effects on unsteady MHD flow over an inclined porous plate embedded in porous medium has been studied. The dimensionless governing equations are solved using finite element method. The obtained results were compared with previous work Pandya and Shukla [9] we found to be good in agreement. An Increase in the Prandtl number is observed to lead to decrease in temperature boundary layer while increase in the Dufour number, thermal radiation results and Eckert number in increase in the thermal boundary layer. It is observed that an increase in Schmidt number decrease in concentration boundary layer while increase in the Soret number in increase in the concentration boundary layer. The velocity increases with the increase in Dufour number, Soret number, Grashof number and solutal Grashof number. Skin-friction increases when Dufour number and Soret number increase. Nusselt number increases when Dufour number and Soret number increase. Sherwood number decreases as Dufour number and Soret number increase.

References

[1] Ecekert E. R. G, Drake R.M. Analysis of Heat and Mass Transfer. McGraw Hill; 1972.

[2] Z. Dursunkaya, W.M.Worek, Diffusion-thermo and thermal diffusion effects in transient and steady natural convection from a vertical surface. International Journal of Heat and Mass Transfer, Vol. 35 (1992), 2060-2065.

[3] N.G. Kafoussias, N.G. Williams, Thermal diffusion and diffusion-thermo effects on mixed free-forced convective and mass transfer boundary layer flow with temperature dependent viscosity. Int. J. Eng. Sci, Vol. 33 (1995), 1369-1384.

[4] M.S. Alam, M.M. Rahman, A. Maleque, M. Ferdows , Dufour and Soret effects on steady MHD combined free- forced convective and mass transfer flow past a semi-infinite vertical plate. Thammasat International Journal Science Technology, Vol. 11 (2006), 1-12.

[5] D. Srinivasacharya, M. Upendar, Soret and Dufour effects on MHD mixed convection heat and mass transfer in a micropolar fluid. Cent. Eur. J .Eng, Vol. 3 (2013) No. 4, 679-689.

[6] Postelnicu, Influence of a Magnetic field on heat and Mass Transfer by natural convection from vertical surface in porous media considering Soret and Dufour effects. International Journal of Heat and Mass Transfer, Vol.47 (2004) No. 6, 1467-1472.

[7] M. A. Alabraba, A.R. Bestman, A. Ogulu, Laminar convection in binary mixed of Hydro magnetic flow with Radiative Heat Transfer. Astrophysics and Space Science, Vol.195 (1992) No. 2, 431-439.

[8] M.D. Enamul Karim, M.D. Abdus Samad, M.D. Maruf Hasan, Dufour and Soret effect on steady MHD flow in presence of Heat generation and magnetic field past an inclined stretching sheet. Open Journal of Fluid Dynamics, Vol. 2 (2012), 91-100.

[9] N. Pandya, A.K. Shukla, Soret-dufour and radiation effect on unsteady MHD flow over an inclined porous plate embedded in porous medium with viscous dissipation. Int. J. Adv. Appl. Math. And Mech, Vol. 2 (2014) No.1, 107 119.

[10] Siva Reddy Sheri and R Srinivasa Raju, Soret effect on unsteady MHD free convective flow past a semi infinite vertical plate in the presence of viscous dissipation. International Journal for computational methods in engineering Science and Mechanics, Vol. 16 (2015) No.2, 132-141. DOI:10.1080/15502287.2015.1009583

[11] E.M. Sparrow, R. D. Cess, Effect of Magnetic field on free convection heat transfer. Int J Heat Mass Transfer, Vol. 3 (1961), 267-270.

[12] P.V. Satyanarayana, D.Ch. Kesavaiah, S. Venkataramana, Viscous dissipation and thermal radiation effects on Unsteady MHD convection flow past a semi infinite vertical permeable moving porous plate. IJMA, Vol. 2 (2011) No.4, 476-487.

[13] A. Bhattacharya, R.K. Dekab, Radiation and stratification effect on transient free convective flow of an elastico-viscous fluid

past an infinite vertical plate. International Journal of Applied Mathematics and Computation, Vol. 5 (2013) No.2, 1827.

[14] Khem chanda, Sanjeev Kumar, Effect of Hall current and rotation on chemically reacting and radiating MHD oscillatory dusty viscoelastic flow through porous vertical channel. International Journal of Applied Mathematics and Computation, Vol. 5 (2013) No.3, 1732.

[15] S Shivaiah, J Anand Rao, Effects of Soret Dufour and Thermal radiation on an unsteady MHD free convection flow past an infinite vertical porous plate in the presence of chemical reaction. International Journal of Applied Mathematics and Mechanics, Vol. 7 (2011), No. 13, 58-76.

[16] S.Sivaiah, MHD Flow of a Rotating Fluid Past a Vertical Porous Flat Plate in the Presence of Chemical Reaction and Radiation. Journal of Engineering Physics and Thermo physics, Vol. 86 (2013), No.6, 1328-1336.

[17] Dr. S. Ravi Kumar, The Effect of the Couple Stress Fluid Flow on MHD Peristaltic Motion with Uniform Porous Medium in the Presence of Slip Effect. Jordan Journal of Mechanical and Industrial Engineering, Vol. 9 (2015), No. 4, 269 278.

[18] Subodh Kumar Sharma, Parveen Kumar Saini, Narendra Kumar Samria, Computational Modeling of Temperature Field and Heat Transfer Analysis for the Piston of Diesel Engine with and without Air Cavity. Jordan Journal of Mechanical and Industrial Engineering, Vol. 9 (2015), No. 2, 139 147.

[19] E.M. Sparrow, R.D. Cess, Temperature dependent heat sources or sinks in a stagnation point flow. Appl. Sci. Res, Vol.10 (1961), 185-197.

[20] A. J Chamkha, A.R.A Khaled, Similarity solutions for hydromagnetic simultaneous heat and mass transfer by natural convection from an inclined plate with internal heat generation or absorption. Heat Mass Transfer, Vol. 37 (2001), 117-123.

[21] B.K. Jha, A.O. Ajibade, Free convective flow of heat generating/absorbing fluid between vertical porous plates with

periodic heat input. Int. Comm. Heat Mass Transfer, Vol.36 (2009), 624-631.

[22] Bathe K.J. Finite Element Procedures. New Jersey: Prentice-Hall; 1996.

[23] Reddy J.N. An Introduction to the Finite Element Method. 3rd Edition. New York: McGraw-Hill Book Company; 2006.